Structural Determinants for Plant Annexin−Membrane Interactions†

Nicole Dabitz,‡,§ Nien-Jen Hu,§,|| Adlina Mohd Yusof,|| Nicola Tranter,|| Anja Winter,|| Marc Daley,|| Olaf Zschörnig,‡ Alain Brisson,⊥ and Andreas Hofmann*,||

Institut für Medizinische Physik und Biophysik, Universität Leipzig, Leipzig, Germany, Institute of Structural and Molecular Biology, School of Biological Sciences, The University of Edinburgh, Scotland, U.K., and Institut Européen de Chimie et Biologie, Université Bordeaux 1, Talence, France

Received August 15, 2005; Revised Manuscript Received October 11, 2005

ABSTRACT: The interactions of two plant annexins, annexin 24(Ca32) from *Capsicum annuum* and annexin Gh1 from *Gossypium hirsutum*, with phospholipid membranes have been characterized using liposome-based assays and adsorption to monolayers. These two plant annexins show a preference for phosphatidylserine-containing membranes and display a membrane binding behavior with a half-maximum calcium concentration in the sub-millimolar range. Surprisingly, the two plant annexins also display calcium-independent membrane binding at levels of 10−20% at neutral pH. This binding is regulated by three conserved surface-exposed residues on the convex side of the proteins that play a pivotal role in membrane binding. Due to quantitative differences in the membrane binding behavior of N-terminally His-tagged and wild-type annexin 24(Ca32), we conclude that the N-terminal domain of plant annexins plays an important role, reminiscent of the findings in their mammalian counterparts. Experiments elucidating plant annexin-mediated membrane aggregation and fusion, as well as the effect of these proteins on membrane surface hydrophobicity, agree with findings from the membrane binding experiments. Results from electron microscopy reveal elongated rodlike assemblies of plant annexins in the membrane-bound state. It is possible that these structures consist of protein molecules directly interacting with the membrane surface and molecules that are membrane-associated but not in direct contact with the phospholipids. The rodlike structures would also agree with the complex data from intrinsic protein fluorescence. The tubular lipid extensions suggest a role in the membrane cytoskeleton scaffolding or exocytotic processes. Overall, this study demonstrates the importance of subtle changes in an otherwise conserved annexin fold where these two plant annexins possess distinct modalities compared to mammalian and other nonplant annexins.

Although plant annexins share many structural, biochemical, and histological properties with their animal homologues (*1*−*4*), they also display distinct differences (for a review, see ref *5*). The typical annexin fold, present in all annexins investigated thus far, comprises an N-terminal tail of variable length and a 4-fold repeat of a 70-amino acid sequence which constitutes the four domains of the C-terminal core. Each of the four compact domains (I−IV) consists of a four-helix bundle (A, B, D, and E) where the helices are arranged in an approximately (anti-) parallel fashion. A fifth helix (C) is oriented almost perpendicular to the bundle. The canonical calcium binding site in annexins is provided by the endonexin sequence which is missing in the plant homologues in domains II and III.

Although there have been studies concerned with plant annexin−membrane binding, an in-depth analysis of the interactions at the molecular level has not been performed. We know to date that plant annexins bind to phospholipid membranes in a calcium-dependent manner (*4*, *6*−*11*), and some of the proteins are involved in membrane aggregation (*9*, *10*). The natural membrane systems investigated include secretory vesicles (*9*), plasma membranes, and microsomal vesicles (*6*). Two annexin-like proteins from *Triticum aestivum* (wheat), p23 and p39, have been characterized as intrinsic membrane proteins due to their biochemical behavior (*6*). Studies using artificial membrane systems agree about the requirement of PS[1] for plant annexin−membrane binding. Binding studies with maize annexin p35 and liposomes composed of PC/PS (1:1) examined the calcium requirements for membrane binding at pH values between 6 and 8 (*8*). Binding at physiological calcium concentrations was only reported for pH 6. Although the half-maximum calcium concentrations for maize annexins p23, p33, and p35 are said to be 20−50 μM, this parameter has been found to be in the sub-millimolar range for bell pepper annexin 24(Ca32) (*7*). On the basis of a mutagenesis study with tomato annexin Le35 (*11*) and a comparison of annexin crystal structures (*12*), it seems clear that only the AB loops of domains I and IV in plant annexins can provide canonical calcium binding sites.

† This study was supported by the Nuffield Foundation (Award to Newly Appointed Lecturers). Richard Denton was the recipient of a BBSRC summer studentship.

* To whom correspondence should be addressed. Telephone: +44 131-650-5365. Fax: +44 131-650-8650. E-mail: Andreas.Hofmann@ed.ac.uk.

‡ Universität Leipzig.

§ These authors contributed equally to this work.

|| The University of Edinburgh.

⊥ Université Bordeaux 1.

[1] Abbreviations: DOPC, dioleoylphosphatidylcholine; DOPS, dioleoylphosphatidylserine; PC, phosphatidylcholine; PE, phosphatidylethanolamine; PS, phosphatidylserine.

10.1021/bi0516226 CCC: $30.25
Published on Web 11/16/2005

The calcium-dependent binding of annexins to phospholipid membranes and the annexin-mediated effects on these membranes have been a subject of intense research for ~20 years. Many groups have devised liposomes as the model membrane of choice, and an enormous variety of different assays have been developed (*13*). In the study presented here, we aim to characterize plant annexin−membrane binding with a variety of liposome-based assays utilizing bell pepper annexin 24(Ca32) and cotton annexin Gh1 as models. We also conducted surface-film balance measurements and electron microscopy of membrane-bound plant annexins. The role of particular surface residues has been tested through annexin mutants generated by site-directed mutagenesis based on the crystal structures reported by us (*7*, *14*).

EXPERIMENTAL PROCEDURES

Cloning, Expression, and Purification of Recombinant Proteins. The mutant proteins used in this study carry an N-terminal His_n fusion peptide and were cloned as described previously (*7*, *15*). Annexin 24 mutants were produced by subjecting the His-tagged Anx24(Ca32) construct to site-directed mutagenesis (*16*). Expression and purification of His-tagged plant annexins have been described previously (*7*, *15*). Untagged protein was purified by calcium-dependent binding to liposomes made from bovine spinal cord extract (Lipid Products, Surrey, U.K.) and subsequent anion exchange chromatography on a Q-Sepharose column. Annexin A5 was used as a control and purified as described previously (*17*). All proteins used within this study were more than 95% pure as assessed by SDS−PAGE.

Membrane Binding Assay (Copelleting Assay). Phospholipid vesicles were prepared following the protocol of Reeves and Dowben (*18*). To assess the plant annexin−membrane binding behavior, a copelleting assay was conducted (*13*). A total amount of 0.2 μmol of phospholipids was used for each individual sample (500 μL), composed of 0.5 nmol of protein in liposome buffer and varying amounts of calcium. As a control, a sample of 0.1 nmol of protein in 100 μL of 10% SDS was prepared at this stage. All samples were centrifuged (23 000 rpm at 4 °C for 45 min), and the pellets were resuspended with 50 μL of 10% SDS and then subjected to SDS−PAGE. Gels were stained with Coomassie and analyzed densitometrically using ImageJ (*19*). Each calcium concentration was assessed three times independently. Curve fitting was performed with SigmaPlot using a standard binding equation.

Surface Film Balance Experiments. Kinetic studies of binding of plant annexin to membrane monolayers were carried out using a computer-controlled Langmuir film balance (NIMA) at 20 °C. The subphase buffer contained 160 mM NaCl and 10 mM HEPES (pH 7.4). During the experiment, a Teflon stirrer was run at a rotation frequency of 6 rpm. The lateral surface pressure, π, was measured with a surface potential meter using plates (1 cm × 2.3 cm) cut from filter paper (Whatman, No. 1). The lipid solution was prepared as a 3:1 mixture of 1,2-dimyristoyl-*sn*-glycero-3-phosphocholine (DMPC) and 1,2-dimyristoyl-*sn*-glycero-3-phosphoserine (DMPS) from the phospholipid solutions in chloroform (1 mg/mL). The lipid monolayer was spread by applying 30 μL of the mixture onto the surface of the subphase with a Hamilton microsyringe. The phospholipid monolayer was considered to be equilibrated when the lateral surface pressure maintained a stable baseline (usually after 20 min). The thin film was then compressed to an initial lateral surface pressure of ~16−20 mN/m (*20*) and equilibrated again to reach a stable baseline (usually in 5 min), after which the protein solution was injected into the subphase with a Hamilton microsyringe extending beneath the barrier. The lateral surface pressure, π, was recorded versus time until no further increase in pressure was observed.

Phospholipid Vesicle Preparation. For experiments assessing membrane surface hydrophobicity, liposome leakage, vesicle size, and vesicle fusion, the following protocols were used. Brain phosphatidylserine (PS), egg phosphatidylcholine (PC), egg phosphatidylethanolamine (PE), nitrobenzoxadiazole phosphatidylethanolamine (NBD-PE), and lissamine rhodamine B sulfonyl phosphatidylethanolamine (Rh-PE) were from Avanti Polar Lipids (Alabaster, AL). Multilamellar phospholipid vesicles (MLVs) were prepared using the method of Bangham (*21*). The MLVs were converted into large unilamellar vesicles (LUVs) by five freeze−thaw cycles and subsequent extrusion (five times) through 0.1 μm Nucleopore filter membranes using an extruder (Lipex Biomembranes, Vancouver, BC) at 30 °C. Phosphate determination was performed according to the method of Chen and co-workers (*22*).

Membrane Surface Hydrophobicity. An increase in membrane surface hydrophobicity is the result of dehydration of the phospholipid headgroups by either the binding of protein to the membrane surface or the creation of water-free interfaces between two vesicles, which occurs during aggregation. Changing membrane surface hydrophobicity can be observed by labeling vesicles with *N*-[5-(dimethylamino)-naphthalene-2-sulfonyl)-1,2-dioleoylyl-*sn*-glycero-3-PE (dansyl-PE), whose emission wavelength is proportional to the dielectric constant of the probe environment. In this context, pure PS, PS/PE (3:1), and PS/PC (1:1) LUVs containing 1 mol % dansyl-PE were prepared and added to a 900 μL buffer solution (final phospholipid concentration of 45 μM). The effect of annexin on these vesicles was observed at different pH values by injecting 200 nM (0.18 nmol) protein into the calcium-free sample. The samples were excited at 340 nm, and the fluorescence emission was recorded from 400 to 600 nm (*23*). The calcium-dependent behavior of surface hydrophobicity was observed after monitoring the effect of protein alone.

Liposome Leakage Assay. Annexin−phospholipid interactions may cause the destabilization of phospholipid vesicles which results in leakage of the vesicle's interior. In this study, vesicle leakage was monitored by the fluorescence quenching of 8-aminonaphthalene-1,3,6-trisulfonic acid (ANTS) in the presence of *p*-xylen-bis-pyridiniumbromid (DPX). The water-soluble fluorophore ANTS and its quencher DPX were added to the buffer solution while the vesicles were prepared. Excess ANTS/DPX buffer solution was removed by gel filtration using a Sephadex G-50 column. In the undisturbed vesicles, the fluorophore and quencher are spatially close so that DPX quenches the fluorescence of ANTS. With an increasing level of vesicle leakage, ANTS and DPX are diluted into the outer buffer solution, resulting in an increase in the fluorescence of ANTS (*24*).

Photon Correlation Spectroscopy (PCS, dynamic light scattering). PCS was used to determine the average vesicle size in solution which is directly correlated with the degree of aggregation. To obtain an appropriate scattering signal, large amounts of phospholipids were used for these experiments. The calcium-dependent behavior of 250 μM phospholipid in 400 μL of buffer solution was investigated at 25 °C. In the absence and presence of 1 nmol of annexin, the aggregation of the vesicles was observed using a Zetasizer 4 (Malvern Instruments Ltd.) with a He−Ne laser ($\lambda = 632.8$ nm) as the light-emitting source. While the phospholipid:protein ratio was the same as in the phospholipid mixing assay (see Fusion Experiments), the concentration of phospholipids was 5.5-fold higher to obtain a sufficient scattering signal.

Fusion Experiments. Fluorescence energy transfer between NBD-PE and Rh-PE is the basis for an intermixing assay for monitoring the fusion (or hemifusion) of phospholipid layers of two liposome populations (*25*). The labeled population contained 1 mol % NBD-PE and 1 mol % Rh-PE, mixed at a ratio of 1:2 with unlabeled liposomes. Phospholipid mixing of pure PS LUVs, PS/PE (3:1) LUVs, or PS/PC (1:1) LUVs in 900 μL of buffer solution (final phospholipid concentration of 45 μM) was studied in the absence and presence of 200 nM (0.18 nmol) annexin. This was performed by monitoring the fluorescence emission intensity ratio of NBD-PE ($\lambda_{em} = 520$ nm) and Rh-PE ($\lambda_{em} = 588$ nm) using an excitation wavelength of 465 nm. As mixing of the phospholipids occurs, the fluorescence dyes are diluted into larger areas of membrane surface which leads to an increase in the fluorescence emission ratio (*23*).

Intrinsic Protein Fluorescence. Fluorescence emission of Trp35, Trp88, and Trp107 in His_6-Anx24(Ca32), Trp107 in His_6-Anx24(Ca32)-W35A/W88F, and Trp32, Trp85, and Trp104 in His_4-Anx(Gh1) was monitored in the presence and absence of liposomes and calcium at various pH values. Samples consisted of 0.5 μM (0.45 nmol) His_6-Anx24(Ca32), 1.5 μM (1.35 nmol) His_6-Anx24(Ca32)-W35A/W88F, and 0.5 μM (0.45 nmol) His_4-Anx(Gh1) each in 900 μL of buffer solution. The samples were excited at 295 nm, and emission was recorded from 315 to 400 nm using a FluoroMax-2 spectrofluorimeter (Jobin-Yvon).

Electron Microscopy (EM). Two-dimensional (2D) crystallization experiments were conducted following the protocol described by Brisson and colleagues (*26*). Incubation times for crystallization varied between 30 min and overnight. The crystalline material present at the air−water interface was transferred onto EM grids coated with a perforated carbon film by the horizontal lifting method (*27*), negatively stained with 1% uranyl acetate, and coated with a thin layer of carbon to increase their stability. EM observations were performed with a Philips CM120 instrument operating at 120 kV, equipped with a 1K × 1K Gatan-794 slow-scan CCD camera which has a step size of 0.24 μm. Electron micrographs of negatively stained samples were recorded under low-dose conditions. Images were processed using an ensemble of modified MRC (*28*) packages.

RESULTS

Membrane Binding Behavior. As shown in Figure 1A (also Table 1), the His_n-tagged wild-type plant annexins exhibit a

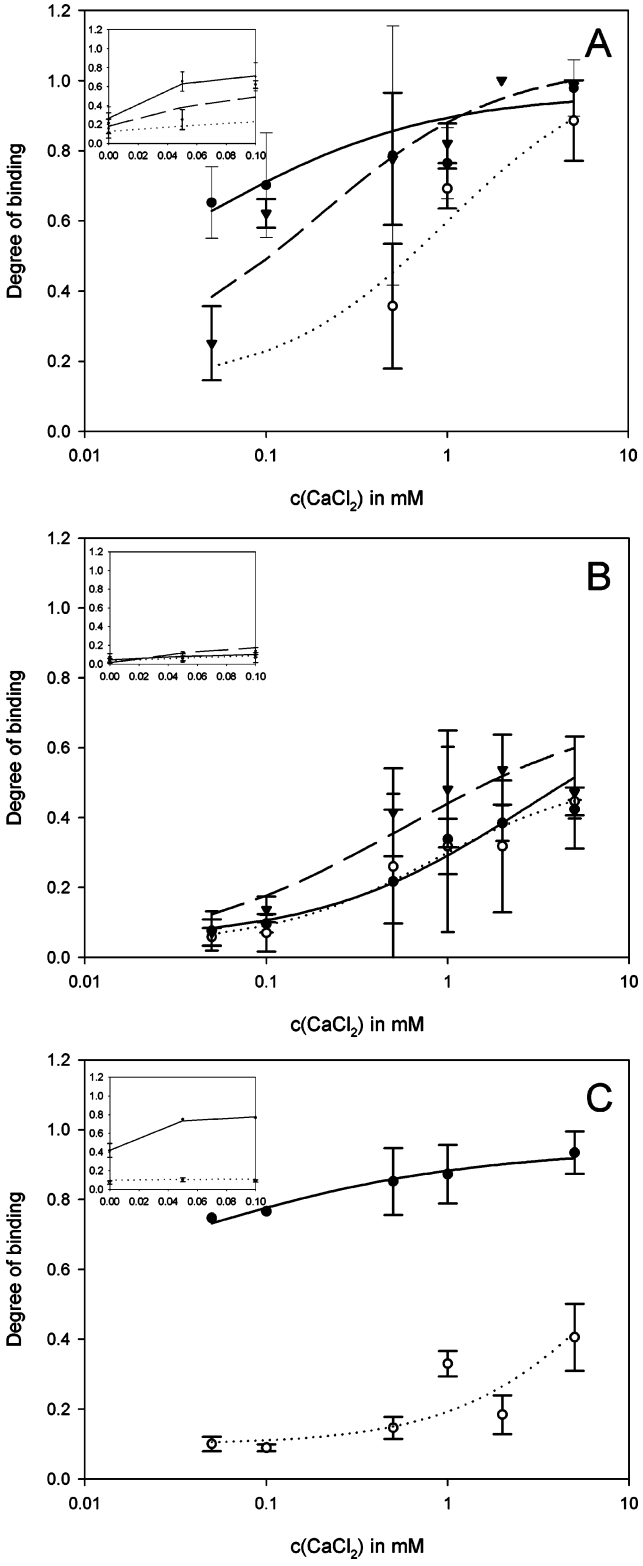

FIGURE 1: Copelleting assay of annexin 24(Ca32) and annexin Gh1. Data points represent the average of at least three independent experiments. Data were fitted with a standard binding equation (Hill coefficient $n = 1$). The degree of membrane binding at $c(Ca^{2+}) = 0$ can be seen in the linear plots (insets). (A) Calcium-dependent membrane binding curves for wild-type annexins: His_6-Anx24-(Ca32) (●), untagged Anx24(Ca32) (○), and His_4-Anx(Gh1) (▼). (B) Calcium-dependent membrane binding curves for tryptophan mutant bell pepper annexins: His_6-Anx24(Ca32)-W35A/W88F (●), His_6-Anx24(Ca32)-W35G (○), and His_6-Anx24(Ca32)-W107G (▼). (C) Calcium-dependent membrane binding curves for basic surface residue mutants: His_6-Anx24(Ca32)-R262A/R263A (●) and His_6-Anx24(Ca32)-K190G (○).

Table 1: Copelleting Assay

protein	$c_{1/2}$-(Ca^{2+})	binding at $c(Ca^{2+}) = 0$ (%)	maximal binding (%)
Anx24(Ca32)	0.65 mM	13	99[a]
His_6-Anx24(Ca32)	0.03 mM	27	94[b]
His_6-Anx24(Ca32)-W35A/W88F	0.4 mM	4	67[a]
His_6-Anx24(Ca32)-W35G	0.7 mM	4	53[a]
His_6-Anx24(Ca32)-W107G	0.4 mM	3	72[a]
His_6-Anx24(Ca32)-R262A/R263A	0.1 μM	42	92[b]
His_6-Anx24(Ca32)-K190G	3.9 mM	10	74[a]
His_4-Anx(Gh1)	0.11 mM	18	100[b]

[a] Determined at $c(Ca^{2+}) = 20$ mM. [b] Determined at $c(Ca^{2+}) = 5$ mM.

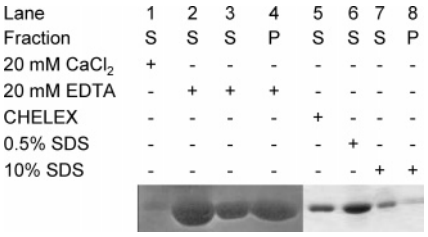

FIGURE 2: Membrane binding behavior of Anx24(Ca32). Shown are Coomassie-stained SDS−PAGE bands from different adsorption or desorption steps of untagged Anx24(Ca32) with liposomes made from bovine brain extract. The protein mixture obtained from the lysis of bacterial spheroblasts was incubated with liposomes in the presence of 20 mM $CaCl_2$. Fraction S is from the supernatant and P from the pellet: lane 1, supernatant of the washing step with 20 mM $CaCl_2$; lane 2, supernatant of the first desorption with 20 mM EDTA; lane 3, supernatant of the second desorption with 20 mM EDTA; lane 4, liposome pellet of the second desorption; lane 5, supernatant of the third desorption using CHELEX; lane 6, supernatant of the washing step with 0.5% SDS; lane 7, supernatant of the washing step with 10% SDS; and lane 8, final liposome pellet.

calcium-dependent membrane binding behavior with a $c_{1/2}(Ca^{2+})$ of 0.03−0.1 mM using PC/PS (3:1) vesicles. The range is on the high side compared to that for mammalian annexins [from 0.6 μM to 0.3 mM (*29*)]. In contrast to mammalian annexins, ~20% of the His-tagged and untagged wild-type plant annexins that were tested bind to the lipid vesicles even in the absence of calcium. This calcium-independent membrane binding differs significantly from the behavior of the mammalian homologues. Qualitatively, this behavior is also obvious from the preparation of plant annexins using the liposome affinity protocol (Figure 2), where a fraction of the protein can be released only in the presence of a detergent (0.5% SDS).

Compared to His_6-Anx24(Ca32), the untagged wild-type Anx24(Ca32) (Figure 1A, dotted line) requires slightly more calcium for half-maximal membrane binding [$c_{1/2}(Ca^{2+}) = 0.7$ mM]. This indicates that the artificial elongation of the N-terminal domain of these plant annexins does affect their membrane binding properties to a certain extent.

To identify key residues for membrane binding, several mutant proteins with altered surface residues were tested. The mutant series was constructed with bell pepper annexin 24 on the basis of analyses of the crystal structures (*7*, *14*), and all mutants carry the N-terminal His_6 tag. The mutant His_6-Anx24(Ca32)-W35G was subjected to the copelleting assay in an effort to elucidate the effects of the conserved tryptophan residue within the first domain. As seen in Figure 1B, this mutant shows a significantly reduced calcium-dependent membrane binding activity. Furthermore, it has also lost the ability to attach to membranes in a calcium-independent manner. A double mutant, His_6-Anx24(Ca32)-W35A/W88F, originally constructed to perform fluorescence experiments using the remaining Trp107 as an intrinsic probe, was also tested in the copelleting assay and found to behave in a manner similar to that of His_6-Anx24(Ca32)-W35G (Figure 1B).

Disabling the second surface-exposed tryptophan residue, Trp107, yields a mutant with membrane binding activity similar to that of W35G and W35A/W88F. All three tryptophan mutants lack calcium-independent binding, and the saturation levels are between 50 and 70% with W107G at the high end of this range (Figure 1B). Other residues identified from the X-ray structures as being potentially important for membrane binding behavior include Lys190 in the third domain, and Arg262 and Arg263 in the fourth domain (Figure 1C). The effect of the latter residues was investigated with a double mutant His_6-Anx24(Ca32)-R262A/R263A which displays membrane binding behavior akin to that of the wild-type His-tagged protein. The saturation level at 5 mM calcium is 92% as compared to 94% for His_6-Anx24(Ca32). Interestingly, the level of calcium-independent membrane binding is approximately twice as high as that of the wild-type protein. In contrast, changing Lys190 to glycine severely disrupts the membrane binding activity of the protein. This mutant possesses the highest half-maximal calcium concentration among all the mutants tested within this study, ~4 mM. Furthermore, the level of calcium-independent membrane binding is decreased to ~10%.

We also attempted to characterize plant annexin membrane binding behavior by surface film measurements, using annexin A5 as a control. Measurements with annexin A5 as reported in this study qualitatively agree with the results from a more detailed investigation of annexin A5 in this context, using DMPA monolayers and different experimental parameters (*30*), as well as with an earlier study by Mukhopadhyay (*20*). Results for the binding of 100 nM annexin A5 (1 mM $CaCl_2$) to a PS/PC (3:1) monolayer exhibit the anticipated binding behavior with an immediate onset when $\pi_0 = 19$ mN/m and $\pi_0 = 20$ mN/m (Figure 3D,E). The saturation level is reached after approximately 30 min, and the increase in surface pressure is as follows: $\Delta\pi = 3$ mN/m ($\pi_0 = 19$ mN/m) and $\Delta\pi = 2.5$ mN/m ($\pi_0 = 20$ mN/m). In contrast, the increase in lateral surface pressure for His_6-Anx24(Ca32) under similar conditions (150 nM protein and 3 mM $CaCl_2$) is not significant (data not shown). However, increasing the protein concentration to 1.5 μM resulted in a binding curve, albeit at a much slower rate (Figure 3B,C). Irrespective of the initial pressure ($\pi_0 = 16$ mN/m or $\pi_0 = 20$ mN/m), the level of saturation is reached after only approximately 85 min. However, the increase in lateral surface pressure is much more pronounced ($\Delta\pi \sim 5$ mN/m) than that observed with the annexin A5 control. Compared to the hexa-His fusion protein, wild-type annexin 24(Ca32) has a less effective membrane adsorption. While the level of saturation is reached after ~45 min, the increase in lateral surface pressure ($\Delta\pi$) elicited by the untagged protein is only 1.3 mN/m.

Membrane binding of selected plant annexin proteins was further characterized by the assessment of protein effects on membrane surface hydrophobicity, vesicle leakage, and vesicle aggregation and/or fusion. In the presence of protein,

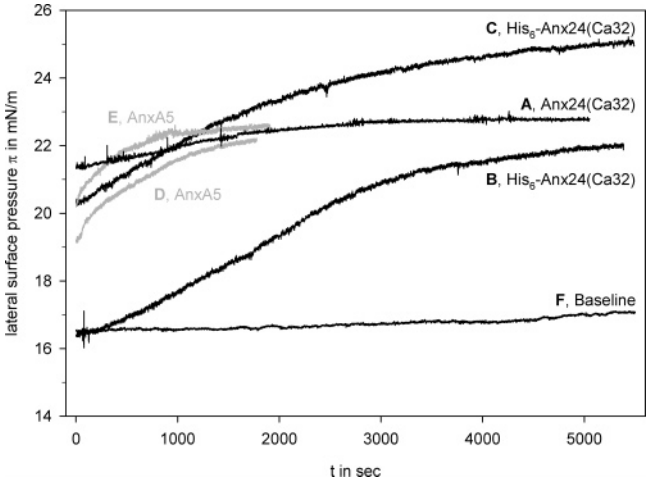

FIGURE 3: Surface film balance measurements with DMPC/DMPS (3:1) monolayers. The subphase contained 160 mM NaCl and 10 mM HEPES (pH 7.4): (A) 1.5 μM Anx24(Ca32), 3 mM $CaCl_2$, $\pi_0 = 20$ mN/m; (B) 1.5 μM His_6-Anx24(Ca32), 3 mM $CaCl_2$, $\pi_0 = 16$ mN/m; (C) 1.5 μM His_6-Anx24(Ca32), 3 mM $CaCl_2$, $\pi_0 = 20$ mN/m; (D) 100 nM AnxA5, 1 mM $CaCl_2$, $\pi_0 = 19$ mN/m; (E) 100 nM AnxA5, 1 mM $CaCl_2$, $\pi_0 = 20$ mN/m; and (F) control experiment without protein, $\pi_0 = 16$ mN/m.

a calcium-dependent increase in hydrophobicity was observed at neutral pH for His_6-Anx24(Ca32), His_6-Anx24-(Ca32)-W35A/W88F, and His_4-Anx(Gh1) for PS and PS/PE (3:1) vesicles but not for PS/PC (1:1) vesicles. In comparison with protein-free control experiments, less calcium was needed to achieve the same degree of hydrophobicity (data not shown).

Vesicle leakage occurs when stress exists in the membrane bilayer and can be provoked by the presence of metal ions, insertion of peptides and proteins into the membrane, or pore formation. At pH 6, calcium-dependent destabilization by His-tagged annexin 24(Ca32) is observed with PS liposomes. While the annexin alone caused ~3% leakage, the level was around 10% at 0.1 mM Ca^{2+} and could not be increased by 0.5 mM Ca^{2+}. A similar behavior at slightly lower leakage levels was seen with PS/PC (1:1) liposomes at pH 6 and 7.4. His_4-Anx(Gh1) exhibited an equivalent calcium-dependent behavior, albeit at higher levels of leakage. At pH 7.4, the cotton annexin caused a level of calcium-independent vesicle leakage of ~20% with PS liposomes. This activity compares very well to the leakage levels observed with annexins A5 and B12 (H. Weigelt, personal communication).

The binding of certain proteins to phospholipid vesicles can promote vesicle aggregation or even fusion. While aggregation describes the spatial vicinity of vesicles mediated by linking protein molecules, vesicle fusion results from direct vesicle−vesicle interactions and leads to a subsequent intermixing of the constituent phospholipids. In this study, vesicle aggregation was monitored by evaluating the vesicle size using light scattering. Meanwhile, vesicle fusion was evaluated by determining the degree of mixing of the constituent phospholipids. Generally, results from the aggregation (vesicle size) and fusion (phospholipid mixing) assays are in excellent agreement throughout. At neutral pH values, His_6-Anx24(Ca32) promotes vesicle aggregation and, to a lesser extent, vesicle fusion in a calcium-dependent manner. Consistently, both effects are more pronounced with PS than with PS/PC (1:1) liposomes. The mutant protein His_6-Anx24(Ca32)-W35A/W88F requires higher calcium concentrations to yield the same extent of vesicle aggregation or fusion as its wild-type counterpart. In contrast, His_4-Anx-(Gh1) requires much higher calcium concentrations than the bell pepper protein.

Intrinsic Protein Fluorescence. Annexin 24(Ca32) possesses three tryptophan residues, Trp35, Trp88, and Trp107. While Trp35 (IAB loop) and Trp107 (IIAB loop) are exposed on the convex side of the molecule, Trp88 is buried in the interior between domains I and II. When the His-tagged protein is exposed to increasing amounts of phospholipid vesicles at pH 6 and 7, the maximum wavelength of tryptophan emission does not vary significantly without calcium (Figure 4A). Upon subsequent addition of calcium, the wavelength of tryptophan emission is almost invariant, irrespective of the composition of the three phospholipid vesicles that were tested (Figure 4B). However, the results for the double mutant W35A/W88F, which has a single remaining tryptophan residue in position 107, are different (Figure 4C). Upon addition of vesicles with high PS content, there is a significant blue shift of 8 nm of the Trp107 fluorescence emission. The subsequent addition of calcium completely reverses this shift. Notably, this behavior is observed only with vesicles having PS contents of 75−100%. The results for vesicles with a PS content of 50% are indistinguishable from the results of the control experiment without liposomes.

Electron Microscopy. Electron microscopy with the His-tagged wild-type annexins Anx24(Ca32) and Anx(Gh1) on lipid monolayers (4:1 DOPC/DOPS) was conducted to investigate possible 2D crystal formation. 2D crystal formation has been observed for some mammalian annexins, including AnxA5 (*31*−*33*) and AnxA6 (*34*−*37*). Other annexins such as AnxA1, AnxA2, and AnxA3 (*39*) do not form 2D crystals. The bell pepper annexin yielded 2D crystals of very poor order with 2 mM $CaCl_2$ present (Figure 5A) and does not present the characteristic diffraction pattern of either the p3 or p6 crystal form. Instead, the crystals look like linear rows presumably made up by annexin dimers. With the cotton annexin, the results improved as particles can be resolved, although there were no homogeneous fields of regular crystals. Intriguingly, elongated rodlike structures that have a tendency to aggregate are observed. The annexin-covered tubes usually have diameters of ~30 nm.

The occurrence of rodlike structures with membrane-bound annexins is not uncommon and is usually explained by the formation of protein-covered lipid tubes on the surface of the lipid monolayer. Since these latter tubes are also hollow, stain is found inside them. However, the annexin-covered lipid tubes usually have smaller diameters of ~140 Å. Thus, it is not clear whether the rodlike structures with larger diameters observed in this study have the same topology. Images such as panels B and C of Figure 5 can also be explained by hollow annexin oligomers adsorbed to the lipid surface. An interesting feature of this structure is the fact that not all protein molecules from the oligomer would be in direct interaction with the membrane surface.

DISCUSSION

From results of this investigation, it is evident that the membrane binding behavior of the tested plant annexins is

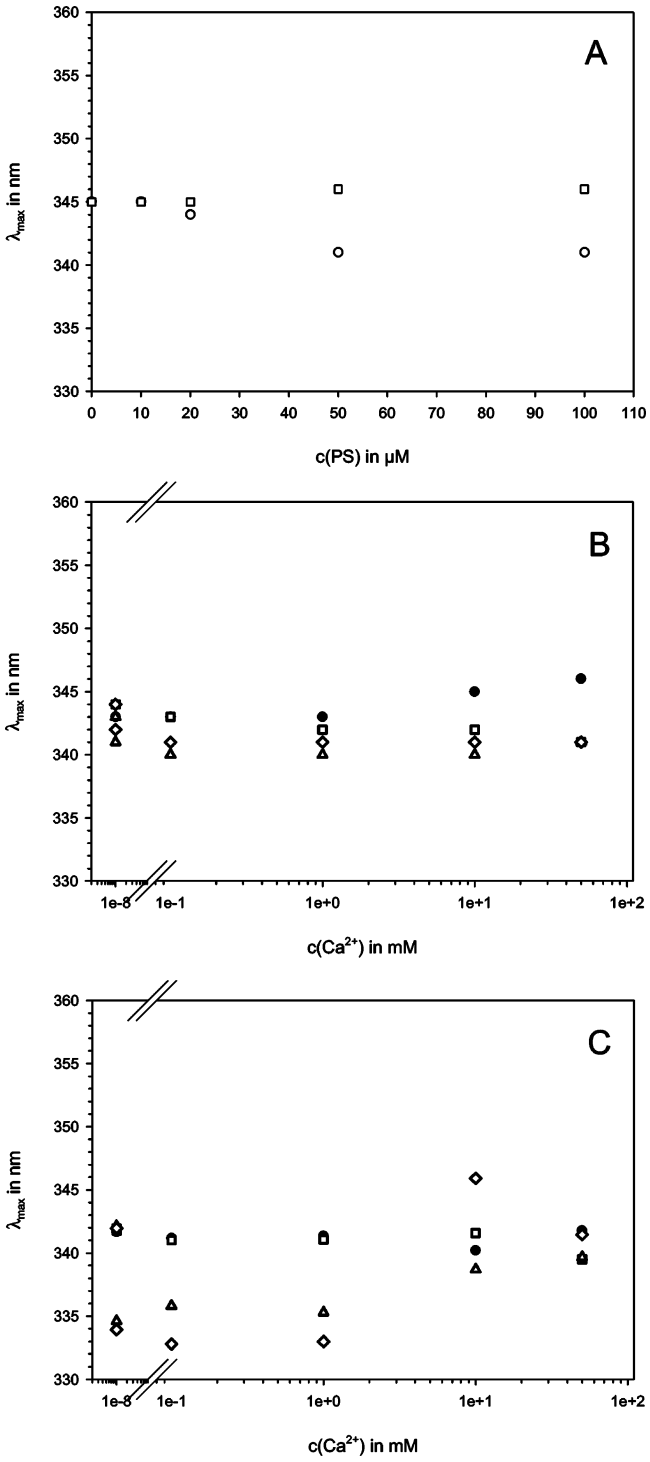

FIGURE 4: Tryptophan fluorescence emission. Data points show the peak wavelength of fluorescence emission spectra of plant annexins at different calcium and PS concentrations. (A) His_6-Anx24(Ca32) (0.5 μM) in varying concentrations of PS liposomes: pH 6 (○) and pH 7.4 (□). (B) His_6-Anx24(Ca32) (0.5 μM) at pH 6 in varying calcium concentrations: without liposomes (●), in the presence of PS/PC (1:1) liposomes (□), with PS/PE (3:1) liposomes (△), and with PS liposomes (◇). (C) His_6-Anx24(Ca32)-W35A/W88F (1.5 μM) at pH 6 in varying calcium concentrations: without liposomes (●), in the presence of PS/PC (1:1) liposomes (□), with PS/PE (3:1) liposomes (△), and with PS liposomes (◇).

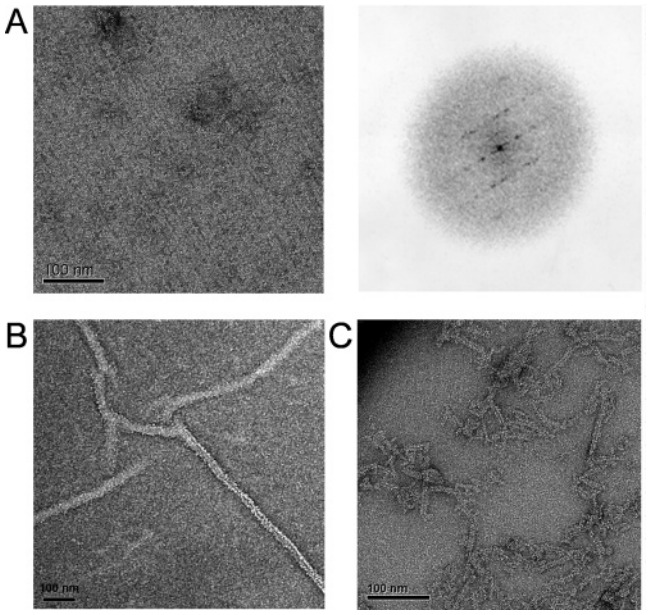

FIGURE 5: Electron microscopy of membrane-bound His-tagged annexin 24(Ca32) and annexin Gh1 on DOPC/DOPS monolayers in the presence of 2 mM $CaCl_2$ (pH 7.4). (A) EM of a 2D crystal of His_6-Anx24(Ca32), and its Fourier transform (inset). (B and C) EM images of membrane-bound His_4-Anx(Gh1) show the formation of rodlike structures that appear to be hollow cylinders associated with the membrane monolayer.

indeed very different from that of their mammalian relatives. Comparison of Langmuir surface film balance measurements for bell pepper annexin 24 and human annexin A5 reveals that at the same calcium concentrations, much more plant protein is required to elicit a similar increase in the lateral surface pressure. At the same time, the adsorption kinetics indicate a much slower association of the plant protein.

It is clearly noted that a major part of this study has been conducted with N-terminally His-tagged annexin proteins. A comparison of the membrane binding behavior of the His fusion proteins with its wild-type counterpart reveals that the N-terminal modification does quantitatively affect the membrane binding behavior. This is evident from the half-maximal calcium concentrations, which are 1 order of magnitude lower for the fusion protein (Table 1), as well as the 4-fold higher increase in the lateral surface pressure (Figure 3). At the same time, wild-type and fusion proteins qualitatively show the same binding behavior with similar distinct features as compared to that of nonplant annexins. The results obtained with His-tagged annexin 24 mutants, with respect to the identification of critical surface residues, are therefore extrapolated to be valid for the untagged protein. Nevertheless, the N-terminal domain of the two plant annexins that were studied plays an important role with respect to membrane interaction, similar to the phenomenon observed with mammalian annexins (*12*, *39*, *40*).

In contrast to their mammalian counterparts, the two plant proteins investigated have the distinct property of binding to acidic phospholipid membranes with their C-terminal cores in the absence of calcium at neutral pH. This calcium-independent binding is severely impaired when Lys190 is replaced with glycine and completely abolished when either Trp35 or Trp107 is disabled. Therefore, it is most likely that the concerted action of (at least) these three surface-exposed residues is responsible for the calcium-independent membrane binding. Importantly, while Trp35 and Lys190 are strictly conserved, Trp107 is conserved in most, but not all, plant annexins. One could therefore speculate that plant

annexins lacking this residue possess a reduced calcium-independent membrane binding activity, although this hypothesis awaits experimental proof. In this context, a second aspect seems to merit attention. The maximum degree of binding, as estimated from the level of saturation, is much lower for mutants W35G, W35A/W88F, W107G, and K190G than for wild-type annexin 24. This suggests that calcium-independent binding is of essential importance for the calcium-dependent binding of these proteins. Since annexin−membrane binding has been described to be highly sequential and displays cooperativity with respect to calcium (*41*, *42*), it is difficult to resolve the exact order of events in the membrane-bound state. However, this study undoubtedly reveals two different binding modes for the tested plant annexins, a calcium-independent and a calcium-dependent mode, which are probably interconnected. The situation is further complicated by the existence of plant annexin oligomers in solution (*15*) which will affect the equilibrium between the soluble and membrane-bound states.

The calcium requirements for membrane binding observed in this study are rather high, thus separating the tested plant annexins from other members in the plant annexin family whose membrane interactions seem to be affected by nanomolar concentrations of calcium (*43*). Notably, these latter experiments were carried out in intact plant cells. The K190G mutant is significantly different in the calcium-dependent binding behavior as its half-maximum calcium concentration is 1 order of magnitude higher than those of the other proteins that were tested. Since Lys190 is not directly involved in any calcium binding event, we believe that this effect is due to either the interplay of conformations on the convex surface or the involvement of this residue in protein−protein interactions that might also affect calcium binding.

On the basis of the crystal structure, a role for residues Arg262 and Arg263 in membrane binding has been anticipated, although results from this study indicate otherwise. The double mutant R262A/R263A has a membrane binding behavior qualitatively similar to that of the wild-type molecule. However, the level of calcium-independent membrane binding is twice as high as that of the wild-type protein, and the half-maximal calcium concentration is decreased by 3 orders of magnitude. With respect to calcium-dependent binding, the presence of two positively charged residues presents a repelling force that restricts the binding of a calcium ion in the IVAB loop. This scenario adds to the fact that the IVAB loop is also capable of coordinating a calcium ion. It remains unclear at this point why the calcium-independent binding of this mutant is enhanced, since a rather favorable interaction of the arginine side chains with either the phospholipid headgroups or the glycerol backbone of the lipid membrane is lost in the mutant. One can speculate that the two arginine residues could be involved in protein−protein interactions and their mutation might give rise to a different species, which interacts with membrane surfaces more readily than the wild-type molecule. The hypothesis merits particular attention, since plant annexins exist as multiple oligomeric species in solution (ref *15* and unpublished results of M. Daley et al.). Also, in contrast to the other wild-type and mutant proteins used in this study, the R262A/R263A mutant readily forms high-molecular weight aggregates (M. Daley and A. Hofmann, unpublished results). Therefore, the binding of this protein to membrane vesicles might be enhanced by unspecific interactions due to the size of the aggregates. It is obvious from the crystal structure of annexin 24 (*7*) that Arg262 and Arg263 are residues in a positive patch on the convex surface of the fourth domain which, apparently, regulates annexin−annexin repulsion.

Assays for assessing phospholipid mixing, vesicle size, and liposome leakage were employed to confirm the interactions between the proteins and lipid vesicles. The data obtained are in excellent agreement with the membrane binding activity determined by the copelleting assay. Results from assays assessing phospholipid mixing and vesicle sizes demonstrate that His-tagged annexin 24(Ca32) promotes the fusion of phospholipid vesicles in a calcium-dependent fashion at neutral pH but only at sufficiently high PS contents. Results for the mutant His_6-Anx24(Ca32)-W35A/W88F concur well with findings from the copelleting experiments and emphasize the crucial role of Trp35 for the membrane binding process. In comparison, His-tagged cotton annexin Anx(Gh1) promotes vesicle aggregation and fusion at much lower levels than the bell pepper protein.

The data acquired from the tryptophan fluorescence emission upon membrane binding are complex. The crystal structures and the fluorescence results agree that the two tryptophan residues, Trp35 and Trp107, are surface-exposed. If the two residues do not reach further than the glycerol backbone area of the phospholipid membrane upon peripheral membrane binding, no significant blue shift of the fluorophores is expected due to the polar nature of this area (*44*). With the bell pepper annexin, the tryptophan emission wavelength is invariant upon calcium-dependent binding of the plant protein in near-neutral environments (pH 6). This can be explained by a model in which not all membrane-associated annexin molecules are actually in direct contact with the membrane (see the discussion of EM results below). The molecules facing the solvent with their convex sides would exhibit fluorescence properties similar to those of the molecules in solution. The superposition of both species would render the fluorescence emission almost invariant. Alternatively, the superposition of one red-shifted and one blue-shifted tryptophan species per molecule would also result in an invariant emission peak, if the two wavelength shifts are small. Interestingly, mutant W35A/W88F, which allows selective monitoring of the residue Trp107, does show a blue shift under the same conditions if the PS content in the membrane vesicles is sufficiently high (>50%). Since Trp107 is positioned in the highest area of curvature on the convex side, it might be able to reach further into the phospholipid membrane than Trp35, which is comparable to the unique Trp187 in annexin A5. The observed red shift of Trp107 from the double mutant W35A/W88F indicates a significant conformational change of the IIAB loop upon calcium-dependent membrane binding. This might happen either by a local conformational change in the IIAB loop retracting the tryptophan side chain from the membrane-embedded position or by the tilting of the entire protein molecule with respect to its initial orientation. Alternatively, a stronger recruitment of protein molecules to the membrane, which associate with the bound molecules but do not directly interact with the membrane surface, could lead to a similar result. However, it cannot be ruled out that a mutant dysfunctional at Trp35 invokes different molecular events

than the wild type molecule. At this stage, structural details of this phenomenon can only be hypothesised and need to be further investigated.

So far, our attempts to produce membrane-bound 2D crystals of plant annexins have not been successful. Instead, we have frequently observed long hollow cylinders of membrane-bound plant annexins. Compared to their mammalian counterparts that do form 2D crystals on membranes, this indicates yet another structural difference in the membrane binding behavior of the plant annexins investigated and their nonplant counterparts. The topology of the observed cylinders requires membrane-associated protein molecules that are not in direct contact with the phospholipids. For such a species to occur, protein−protein interactions are very important, adding further weight to the notion that surface residues other than those on the convex side might be important for the association of plant annexin molecules with the membrane.

In summary, annexins 24 and Gh1, from bell pepper and cotton, respectively, exhibit membrane binding with and without calcium. The calcium-independent binding involves at least three surface-exposed conserved residues on the convex side. Two scenarios can be envisioned. (1) Upon the addition of calcium, the membrane-bound species takes up the ions and utilizes the hypothesised two canonical calcium binding sites for interaction with the membrane surface. (2) Alternatively, calcium-dependent binding occurs in a second species that might or might not be dependent on the calcium-independent species as a platform. It is a generally accepted view for the membrane-bound state of nonplant members of the annexin family that each individual protein molecule interacts directly with the membrane surface. Several indications within this study suggest that this might not be true for plant annexins. Intriguingly, an oligomerization hypothesis has been mentioned for annexin A13b which can be N-terminally myristoylated and plays a role in the apical exocytosis of epithelial kidney cells (*45*). Considering the degree of annexin−annexin interactions in solution and the membrane-bound state, the plant proteins might form extended oligomeric structures that are membrane-associated at one end and may provide another membrane binding site at the other end. Such a structure would be suitable for exocytotic events in which the protein oligomer grabs a membrane vesicle and targets it toward the plasma membrane, in line with the aggregating properties reported for plant annexins in this study. The supramolecular assembly of plant annexins on membrane surfaces might provide a membrane-associated matrix with a scaffolding function which could serve as a platform for binding other proteins.

ACKNOWLEDGMENT

We thank Amy Reeve and Richard Denton for their technical help.

REFERENCES

1. Clark, G. B., Thompson, G., and Roux, S. J. (2001) Signal transduction mechanisms in plants: An overview, *Curr. Sci. 80*, 170−177.
2. Clark, G. B., and Roux, S. J. (1995) Annexins of plant cells, *Plant Physiol. 109*, 1133−1139.
3. Delmer, D. P., and Potikha, T. S. (1997) Structures and functions of annexins in plants, *Cell. Mol. Life Sci. 53*, 546−553.
4. Hoshino, D., Hayashi, A., Temmei, Y., Kanzawa, N., and Tsuchiya, T. (2004) Biochemical and immunohistochemical characterization of *Mimosa* annexin, *Planta 219*, 867−875.
5. Hofmann, A. (2004) Annexins in the plant kingdom: Perspectives and potentials, *Annexins 1*, 51−61.
6. Breton, G., Vazquez-Tello, A., Danyluk, J., and Sarhan, F. (2000) Two novel intrinsic annexins accumulate in wheat membranes in response to low temperature, *Plant Cell Physiol. 41*, 177−184.
7. Hofmann, A., Proust, J., Dorowski, A., Schantz, R., and Huber, R. (2000) Annexin 24 from *Capsicum annuum*. X-ray structure and biochemical characterization, *J. Biol. Chem. 275*, 8072−8082.
8. Blackbourn, H., Walker, J., and Battey, N. (1991) Calcium-dependent phospholipid-binding proteins in plants, *Planta 184*, 67−73.
9. Blackbourn, H. D., and Battey, N. H. (1993) Annexin-mediated secretory vesicle aggregation in plants, *Physiol. Plant. 89*, 27−32.
10. Hoshino, T., Mizutani, A., Chida, M., Hidaka, H., and Mizutani, J. (1995) Plant annexin form homodimer during Ca^{2+}-dependent liposome aggregation, *Biochem. Mol. Biol. Int. 35*, 749−755.
11. Lim, E. K., Roberts, M. R., and Bowles, D. J. (1998) Biochemical characterization of tomato annexin p35: Independence of calcium binding and phosphatase activities, *J. Biol. Chem. 273*, 34920−34925.
12. Hofmann, A., and Huber, R. (2003) Structural conservation and functional versatility: Allostery as a common annexin feature, in *Annexins: Biological importance and annexin-related pathologies* (Bandorowicz-Pikula, J., Ed.) pp 38−60, Landes Bioscience, Georgetown, TX.
13. Hofmann, A., and Huber, R. (2003) Liposomes in assessment of annexin-membrane interactions, *Methods Enzymol. 372*, 186−216.
14. Hofmann, A., Delmer, D. P., and Wlodawer, A. (2003) The crystal structure of annexin Gh1 from *Gossypium hirsutum* reveals an unusual S_3 cluster, *Eur. J. Biochem. 270*, 2557−2564.
15. Hofmann, A., Ruvinov, S., Hess, S., Schantz, R., Delmer, D. P., and Wlodawer, A. (2002) Plant annexins form calcium-independent oligomers in solution, *Protein Sci. 11*, 2033−2040.
16. Jones, D. H., and Howard, B. H. (1990) A rapid method for site-specific mutagenesis and directional subcloning by using the polymerase chain reaction to generate recombinant circles, *BioTechniques 8*, 178−183.
17. Burger, A., Berendes, R., Voges, D., Huber, R., and Demange, P. (1993) A rapid and efficient purification method for recombinant annexin V for biophysical studies, *FEBS Lett. 329*, 25−28.
18. Reeves, J. P., and Dowben, R. M. (1969) Formation and properties of thin-walled phospholipid vesicles, *J. Cell. Physiol. 73*, 49−60.
19. Rasband, W. (2005) *ImageJ*, version 1.30, National Institutes of Health, Bethesda, MD, http://rsb.info.nih.gov/ij/.
20. Mukhopadhyay, S., and Cho, W. (1996) Interactions of annexin V with phospholipid monolayers, *Biochim. Biophys. Acta 1279*, 58−62.
21. Bangham, A. D., Hill, M. W., and Miller, N. G. A. (1974) Preparation and use of liposomes as models of biological membranes, in *Methods in Membrane Biology* (Korn, E. D., Ed.) pp 1−68, Plenum Press, New York.
22. Chen, P. S., Toribara, T. Y., and Warner, H. (1956) Microdetermination of phosphorus, *Anal. Chem. 28*, 1756−1758.
23. Köhler, G., Hering, U., Zschörnig, O., and Arnold, K. (1997) Annexin V interaction with phosphatidylserine-containing vesicles at low and neutral pH, *Biochemistry 36*, 8189−8194.
24. Ellens, H., Bentz, J., and Szoka, F. C. (1985) H^+- and Ca^{2+}-induced fusion and destabilization of liposomes, *Biochemistry 24*, 3099−3106.
25. Müller, M., Zschörnig, O., Ohki, S., and Arnold, K. (2003) Fusion, leakage and surface hydrophobicity of vesicles containing phosphoinositides: Influence of steric and electrostatic effects, *J. Membr. Biol. 192*, 33−43.
26. Brisson, A., Bergsma-Schutter, W., Oling, F., Lambert, O., and Reviakine, I. (1999) Two-dimensional crystallization of proteins on lipid monolayers at the air−water interface and transfer to an electron microscopy grid, *J. Cryst. Growth 196*, 456−470.
27. Langmuir, I., and Schaefer, V. J. (1938) Activities of urease and pepsin monolayers, *J. Am. Chem. Soc. 60*, 1351−1360.
28. Crowther, R. A., Henderson, R., and Smith, J. M. (1996) MRC image processing programmes, *J. Struct. Biol. 116*, 9−16.
29. Blackwood, R., and Ernst, J. (1990) Characterization of Ca^{2+}-dependent phospholipid binding, vesicle aggregartion and membrane fusion by annexins, *Biochem. J. 266*, 195−200.

30. Wu, F., Gericke, A., Flach, C. R., Mealy, T. R., Seaton, B. A., and Mendelsohn, R. (1998) Domain structure and molecular conformation in annexin V/1,2-dimyristoyl-*sn*-glycero-3-phosphate/Ca^{2+} aqueous monolayers: A Brewster angle microscopy/infrared reflection−absorption spectroscopy study, *Biophys. J. 74*, 3273−3281.
31. Mosser, G., Ravanat, C., Freyssinet, J.-M., and Brisson, A. (1991) Sub-domain structure of lipid-bound annexin V resolved by electron image analysis, *J. Mol. Biol. 217*, 241−245.
32. Voges, D., Berendes, R., Burger, A., Demange, P., Baumeister, W., and Huber, R. (1994) Three-dimensional structure of membrane-bound annexin V, a correlative electron microscopy-X-ray crystallography study, *J. Mol. Biol. 238*, 199−213.
33. Oling, F., Bergsma-Schutter, W., and Brisson, A. (2001) Trimers, dimers of trimers, and trimers of trimers are common building blocks of annexin A5 two-dimensional crystals, *J. Struct. Biol. 133*, 55−63.
34. Newman, R. H., Tucker, A., Ferguson, C., Tsernoglou, D., Leonard, K., and Crumpton, M. J. (1989) Crystallisation of p68 on lipid monolayers and as three-dimensional single crystals, *J. Mol. Biol. 206*, 213−219.
35. Gabriel, B. L., Taylor, K., Creutz, C. E., and Kretsinger, R. H. (1991) Microcrystals of the annexin p68: Paracrystal to crystal transition and molecular packing as determined by electron microscopy and image reconstruction, *J. Struct. Biol. 107*, 29−37.
36. Driessen, H. P., Newman, R. H., Freemont, P. S., and Crumpton, M. J. (1992) A model of the structure of human annexin VI bound to lipid monolayers, *FEBS Lett. 306*, 75−79.
37. Benz, J., Bergner, A., Hofmann, A., Demange, P., Gottig, P., Liemann, S., Huber, R., and Voges, D. (1996) The structure of recombinant human annexin VI in crystals and membrane-bound, *J. Mol. Biol. 260*, 638−643.
38. Govorukhina, N., Bergsma-Schutter, W., Mazères-Dubut, C., Mazères, S., Drakopoulou, E., Bystrykh, L., Oling, F., Mukhopadhyay, A., Reviakine, I., Lai Kee Him, J., and Brisson, A. (2003) Self-assembly of annexin A5 on lipid membranes, in *Annexins: Biological importance and annexin-related pathologies* (Bandorowicz-Pikula, J., Ed.) pp 61−78, Landes Bioscience, Georgetown, TX.
39. Ayala-Sanmartin, J., Vincent, M., Sopkova, J., and Gallay, J. (2000) Modulation by Ca^{2+} and by Membrane Binding of the Dynamics of Domain III of Annexin 2 (p36) and the Annexin 2-p11 Complex (p90): Implications for Their Biochemical Properties, *Biochemistry 39*, 15179−15189.
40. Arboledas, D., Olmo, N., Lizarbe, M. A., and Turnay, J. (1997) Role of the N-terminus in the structure and stability of chicken annexin V, *FEBS Lett. 416*, 217−220.
41. Bazzi, M. D., and Nelsestuen, G. L. (1991) Highly sequential binding of protein kinase C and related proteins to membranes, *Biochemistry 30*, 7970−7977.
42. Tait, J. F., Gibson, D. F., and Smith, C. (2004) Measurement of the affinity and cooperativity of annexin V-membrane binding under conditions of low membrane occupancy, *Anal. Biochem. 329*, 112−119.
43. Seals, D. F., Parrish, M. L., and Randall, S. K. (1994) A 42-kilodalton annexin-like protein is associated with plant vacuoles, *Plant Physiol. 106*, 1403−1412.
44. Meers, P. (1990) Location of tryptophans in membrane-bound annexins, *Biochemistry 29*, 3325−3330.
45. Lafont, F., Lecat, S., Verkade, P., and Simons, K. (1998) Annexin XIIIb associates with lipid microdomains to function in apical delivery, *J. Cell Biol. 142*, 1413−1427.

BI0516226